



CHORUS

This is the accepted manuscript made available via CHORUS. The article has been published as:

Thickness of residual wetting film in liquid-liquid displacement

Igor Beresnev, William Gaul, and R. Dennis Vigil

Phys. Rev. E **84**, 026327 — Published 29 August 2011

DOI: [10.1103/PhysRevE.84.026327](https://doi.org/10.1103/PhysRevE.84.026327)

Thickness of Residual Wetting Film in Liquid-Liquid Displacement

By Igor Beresnev^{*}, William Gaul[†], R. Dennis Vigil[†]

^{*} Department of Geological and Atmospheric Sciences, Iowa State University, 253
Science I, Ames, Iowa 50011-3212

[†] Department of Chemical and Biological Engineering, Iowa State University, 2114
Sweeney Hall, Ames, Iowa 50011-2230

Abstract Core-annular flow is common in nature, representing, for example, how streams of oil, surrounded by water, move in petroleum reservoirs. Oil, typically a non-wetting fluid, tends to occupy the middle (core) part of a channel, while water forms a surrounding wall-wetting film. What is the thickness of the wetting film? A classic theory has been in existence for nearly 50 years offering a solution, although in a controversial manner, for moving gas bubbles. On the other hand, an acceptable, experimentally verified theory for a body of one liquid flowing in another has not been available. Here we develop a hydrodynamic, testable theory providing an explicit relationship between the thickness of the wetting film and fluid properties for a blob of one fluid moving in another, with neither phase being gas. In its relationship to the capillary number Ca , the thickness of the film is predicted to be proportional to Ca^2 at lower Ca and to level off at a constant value of about 20 % the channel radius at higher Ca . The thickness of the film is deduced to be approximately unaffected by the viscosity ratio of the fluids. We have conducted our own laboratory experiments and compiled experimental data from other studies, all of which are mutually consistent and confirm the salient features of the theory. At the same time, the classic law, originally deduced for films surrounding moving gas bubbles but often believed to hold for liquids as well, fails to explain the observations.

The Problem

Consider a straight cylindrical capillary channel of small radius filled with a wetting fluid. Subsequently another, non-wetting, fluid begins to flow into the same capillary. This is the scenario of an invasion “core-annular” flow. The non-wetting fluid will tend to occupy the middle part of the channel (the “core”), and the one being displaced will stay adjacent to the channel’s wall as a residual wetting film. How thick is this annular film?

The phenomenon is common in nature. For example, it has long been suggested as a scenario for two-phase immiscible fluid motion through natural porous channels in petroleum reservoirs; it thus describes the movement of oil, as the core phase, through reservoir rock. Despite the apparent simplicity, no adequate, experimentally tested theoretical solutions for the thickness of the wetting film in liquid-liquid displacement, as a function of fluid parameters, have been proposed. The difficulty stems from the fact that the core-annular flow is a “free-boundary” problem, in which the fluid/fluid interface is not fixed but moves and deforms with the flow, with its configuration having to be obtained as part of the solution. Free-boundary fluid-mechanics problems are notoriously difficult to solve (e. g., [Ref. 1, Section 1-1]).

The phenomenon is more easily theoretically described, with some assumptions, if the invading phase is gas. A classic theory of the thickness of an annular film left behind by a retreating pore-filling fluid driven by gas (e. g., air), in the limit of low capillary numbers Ca , was developed by Bretherton [2]. The theory predicted that the thickness of the wetting film, normalized by the channel radius (this dimensionless

thickness will be denoted as b in the following), has a power-law relationship with the capillary number: $b = 1.34 \times Ca^{2/3}$ [Ref. 2, equation 17]. Although the predicted functional form has not truly withstood experimental verification, plausible theoretical explanations for its observed departure from at least a portion of experiments have been offered (see a synopsis of relevant studies in Table 1). Bretherton found a limited agreement with his own experimental data, while noticing the dependence of the observed behavior on a particular wetting fluid used and contradiction of his data with earlier experiments of others [Ref. 2, Figure 4]. Similar experiments repeated a quarter-century later by Schwartz *et al.* [Ref. 3, Figure 3] found a dependence of the residual film thickness and the exponent of the power law on bubble's length, which further departed from Bretherton's predicted behavior. There is general belief that the deviations noted by Bretherton and Schwartz *et al.* in the capillary-number range of $\sim 10^{-5}$ - 10^{-2} are caused by the presence of trace amounts of surfactants and the resulting Marangoni surface flows in the fluids used. For example, Ratulowski and Chang [4] found that an ad-hoc combination of parameters controlling the convective, diffusive, and adsorption effects in a low-concentration surfactant solution (their "convective-equilibrium" asymptotics) is capable of explaining the scatter of experimental relationships reported by Bretherton and Schwartz *et al.* [Ref. 4, Figure 8]. In effect, the free, not experimentally constrained parameters of the model were adjusted to produce a fit to the data. An ad-hoc, albeit plausible, character of this explanation is somewhat unsatisfactory, since there was no guarantee that the required parameter regime was indeed realized in the experiments. Also note that Ratulowski and Chang [4] could not consistently explain the smaller exponent of the power law of $1/2$ at the higher end of their capillary-number range found

by Fairbrother and Stubbs [5], which was found compatible with the measurements of Taylor [6]. Furthermore, Quéré [7] shows that Ratulowski and Chang's predictions are not necessarily compatible with fluid-coating observations. It can be further argued that the departure of Bretherton's theory from experiments might alternatively be explained by the oversimplifications made in the theory, as discussed in a later section in this article.

Despite the not completely satisfactory experimental verification, Bretherton's theory is generally believed to be accurate in its appropriate capillary-number range of $\sim 10^{-5}$ - 10^{-2} , found by Ratulowski and Chang [4], and has been used extensively in the calculation of thicknesses of wetting films left behind by invading gas bubbles in capillary channels.

When the invading phase is gas, with some reservations, this usage is therefore still acceptable. However, Bretherton's theory has often been assumed to equally apply to the films left behind by one fluid displacing another where neither phase is gas (e. g., [Ref. 8, p. 1998; Ref. 9, equation 4.27]) followed Bretherton's theoretical argument and arrived at an identical solution, although the original theory was limited exclusively to the films surrounding moving gas bubbles. Does such a suggestion stand experimental test? Experimental evidence has been scarce, controversial, and not necessarily supportive; we will address limited available data in an appropriate section. Alternative hydrodynamic theories, which would be better compatible with the data, have not been explored. The questions, therefore, are still outstanding: are film thicknesses, deposited on capillary walls, the same for gas bubbles moving in liquids and for bodies of liquids moving in liquids? Is there sufficient theoretical and experimental evidence suggesting that

Bretherton's law necessarily applies to the liquid/liquid invasion? In this paper, we develop a hydrodynamic theory applying to the case of liquid/liquid displacement and test it in a direct laboratory experiment. We also examine existing experimental data in the context of the present results. The conclusion, supported by both the theory and the experiment, is that Bretherton's power law does not apply to liquid-liquid invasion.

Theory

Our theoretical problem deals with a core-annular, incompressible, axisymmetric Poiseuille flow, which allows analytical solution of the Navier-Stokes equations. It is assumed that the Reynolds number is small. When the interface between the core and the annulus deforms, pressure gradients in each phase will generally be different because of the curvature of the interface according to Laplace's law of capillary pressure. One thus needs to begin with a general solution for the two-phase Poiseuille flow in axisymmetric geometry with non-equal pressure gradients in both phases [10]. The boundary conditions to satisfy are no-slip at the channel wall, continuity of velocity at the fluid-fluid interface, and continuity of shear stress at this interface.

In a typical capillary geometry, Bond numbers, expressing the ratio of gravitational to capillary forces, tend to be small (10^{-2} - 10^{-3}) [10, 11]. It is known that core-annular flow with gravity effects can maintain steady state but acquire axial eccentricity [12]. We assume the smallness of Bond number, which allows us to neglect gravity and use an axisymmetric geometry.

It is convenient to cast the analysis in non-dimensional variables. If we designate by asterisks the variables that have dimensions and drop asterisks for their non-dimensional counterparts, the latter are introduced as follows, $r = r^*/R^*$, $x = x^*/R^*$, $\tau = t^*/(\mu_1^*R^*/\sigma^*)$, $p = p^*/(\sigma^*/R^*)$, $Q = Q^*/(\sigma^*R^{*2}/\mu_1^*)$. Here r^* and x^* are the radial and axial coordinates, respectively; t^* is the time, p^* is the pressure, Q^* is the volumetric flow rate, R^* is the radius of the tube, σ^* is the interfacial tension, and μ_1^* is the core dynamic viscosity. The subscripts “1” and “2” denote the variables in the core and the suspending (wetting) fluids, respectively.

The boundary conditions resolve the axial-velocity profiles $u_1^*(r^*, p_{1x}^*, p_{2x}^*)$ and $u_2^*(r^*, p_{1x}^*, p_{2x}^*)$ in the core and the film, respectively, through the pressure gradients p_{1x}^* and p_{2x}^* , where the subscript x^* indicates the derivative with respect to x^* . These solutions are given by Beresnev and Deng [Ref. 10, equations 6], and, for the sake of brevity, we do not reproduce them here. Integration of these profiles over the cross-sections of the core and the annulus gives volume fluxes $Q_1^*(p_{1x}^*, p_{2x}^*)$ and $Q_2^*(p_{1x}^*, p_{2x}^*)$ [Ref. 10, equations 7]. After nondimensionalization, for the straight tube they become

$$Q_1(p_{1x}, p_{2x}) = -\frac{\pi}{2} \kappa^4 \left[\frac{p_{1x}}{4} + \frac{\mu_1^*}{2\mu_2^*} \left(\frac{1}{\kappa^2} - 1 \right) p_{2x} - \frac{\mu_1^*}{\mu_2^*} (p_{1x} - p_{2x}) \ln \kappa \right], \quad (1a)$$

$$Q_2(p_{1x}, p_{2x}) = -\frac{\pi}{2} \frac{\mu_1^*}{\mu_2^*} \kappa^4 \left[\frac{p_{2x}}{4} \left(\frac{1}{\kappa^2} - 1 \right)^2 + \frac{1}{\kappa^2} (p_{1x} - p_{2x}) \left(\frac{1}{2} - \kappa^2 \ln \frac{\sqrt{e}}{\kappa} \right) \right], \quad (1b)$$

where κ is the radial position of the fluid-fluid interface normalized by R^* .

The volume fluxes (1) still contain the unknown pressure gradients; however, Laplace's law supplies another (non-dimensionalized) equation relating p_1 and p_2 :

$$p_1 - p_2 = \frac{1}{\kappa} - \kappa_{xx},$$

where the right-hand side is the dimensionless mean curvature of the interface [Ref. 13, equation 7; Ref. 14, equations 2, A5-A7]. Here we used the assumption of a "small slope" of the interface, which allowed us to neglect the terms κ_x^2 with respect to unity in the full expression for the curvature. The same approach was taken by Bretherton [Ref. 2, equation 4], allowing the use of the solutions for Poiseuille flow. Note, also, that the use of Laplace's law has implied the smallness of the capillary number, which characterizes the ratio of viscous to capillary forces. We therefore neglect the viscous normal stresses in the moving fluid.

The last equation leads to $p_{1x} - p_{2x} = -\frac{\kappa_x}{\kappa^2} - \kappa_{xxx}$. If we combine it with the conservation-of-mass condition $Q_1(p_{1x}, p_{2x}) + Q_2(p_{1x}, p_{2x}) = Q$, where Q is the total volume flux through the tube, the two equations form the system from which both p_{1x} and p_{2x} can be resolved. When substituted them back into Q_1 in equation (1a), this leads to an explicit formula

$$Q_1 = \frac{\mu_2^*}{\mu_1^*} \frac{Q \left[1 + 2 \frac{\mu_1^*}{\mu_2^*} \left(\frac{1}{\kappa^2} - 1 \right) \right]}{\frac{1}{\kappa^4} + \frac{\mu_2^*}{\mu_1^*} - 1} - \frac{\pi}{2} \kappa^2 (\kappa_x + \kappa^2 \kappa_{xxx}) \left\{ \frac{\left(\frac{1}{\kappa^2} - 1 \right) \left[\left(\frac{\mu_1^*}{\mu_2^*} - \frac{1}{4} \right) \frac{1}{\kappa^2} + \frac{3}{4} - \frac{\mu_1^*}{\mu_2^*} \right]}{\frac{1}{\kappa^4} + \frac{\mu_2^*}{\mu_1^*} - 1} + \frac{\mu_1^*}{\mu_2^*} \ln \kappa \right\}. \quad (2)$$

Q_1 described by equation (2) is the volume flux in the core fluid when it moves into the suspending phase that initially fills the capillary tube. Since we are looking for stationary solutions, the front meniscus, separating the two fluids, moves without changing its shape with constant speed U^* . The geometry is illustrated in Figure 1. The core displaces part of the suspending fluid that is ahead of the moving meniscus, leaving part of it behind as a wetting film on the wall. The film thickness, normalized by R^* , is b . In this geometry, conservation of mass requires that Q_1 be also equal to $Q_1 = \pi U(1-b)^2$,

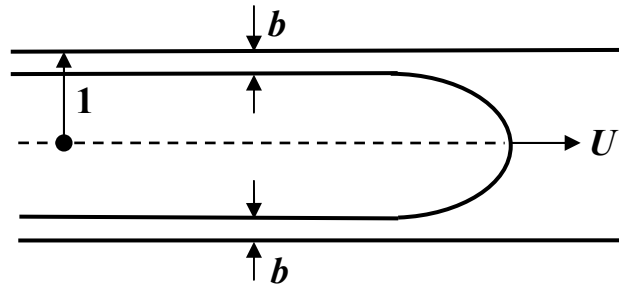


Figure 1. Geometry of the core-fluid invasion.

which is the flow rate of the displaced fluid ahead of the invading core body [Ref. 15, equation 3], where the speed has been non-dimensionalized using $U = U^*/(\sigma^*/\mu_1^*)$. Note that the respective conservation-of-mass condition, used by Bretherton [Ref. 2, equations 7-8] and reproduced by Middleman [Ref. 1, equations 2-4.6 – 2-4.7], inconsistently neglects the flow in the film, whereas Goldsmith and Mason's condition is more general and correct. The last formula, rewritten in terms of the capillary number, $Ca = \mu_2^* U^*/\sigma^* = U\mu_2^*/\mu_1^*$, becomes $Q_1 = \pi \frac{\mu_1^*}{\mu_2^*} Ca(1-b)^2$. Equating this expression for Q_1 with that from equation (2) leads to the differential equation for the wetting-film profile $\kappa(x)$.

The resulting equation is extremely complex and cannot be approached analytically without simplifications. We notice, however, that somewhere near the nose the moving front in Figure 1 has a round (but not necessarily spherical) shape. Following Bretherton [Ref. 2, discussion leading from his equation 11 to 12] (also see [Ref. 1, equations 2-4.10 – 2-4.11]), we seek a simplified form of equation (2) somewhere in the transition zone between the nose of the invading core phase and the residual film, at small values of κ , by retaining only the important terms. At sufficiently small κ , constant terms can be neglected compared to $1/\kappa^2$, $1/\kappa^4$, and $\ln \kappa$. In the same approximation, we can neglect $2Q\kappa^2$ with respect to Q_1 and, assuming a bounded third derivative, $\kappa^2\kappa_{xxx}$ with respect to κ_x . This leads to a simpler form of the film-profile equation,

$-\frac{1}{2}\kappa^2\kappa_x \ln \kappa = Ca(1-b)^2$. The transition to this form and the approximations made are equivalent to Bretherton's numerical solution of his main film-profile equation (11), assuming the asymptotic interface shape near the nose (12), which led to the final equation (17) (this transition is also discussed by Middleman [Ref. 1, equations 2-5.41 – 2-5.45]). Note that the viscosity ratio has dropped out. Rearranging, we write

$$\kappa_x = -\frac{2Ca(1-b)^2}{\kappa^2 \ln \kappa} \text{ and, differentiating one more time,}$$

$$\kappa_{xx} = -\frac{8Ca^2(1-b)^4}{\kappa^5 \ln^2 \kappa}. \quad (3)$$

Formula (3) is valid somewhere in the transition zone. In this region, the meniscus has a round shape, but, because the meniscus is moving, is not exactly a sphere. The

curvature of the sphere would be $2/(1-b)$, and therefore a matching condition

$1/(1-b) - \kappa_{xx} \approx 2/(1-b)$, or $|\kappa_{xx}| \approx 1/(1-b)$, will approximately hold [Ref. 1, equations 2-

4.12 – 2-4.13; Ref. 2, discussion leading from equation 12 to equation 13]. To

approximate the departure from the spherical shape, we add a correction to make the

right-hand side equal $1/(1-b) + C_1$; the value of C_1 is to be determined. Using (3) for κ_{xx}

in the result leads to the equation for b ,

$$b = \frac{C_2(1+C_1) - 8Ca^2}{C_1C_2 - 40Ca^2}, \quad (4)$$

where we approximated $(1-b)^5 \approx 1-5b$ and introduced a notation $C_2 \equiv \kappa^5 \ln^2 \kappa$.

We are now able to constrain the value of C_1 . At small capillary numbers, equation (4) becomes $b = (1+C_1)/C_1$. We immediately see that C_1 cannot be positive or zero, since b , by definition, cannot be greater than one. Also, b must be non-negative, which further constraints C_1 to be $C_1 \leq -1$. Furthermore, the curvature in the right-hand side of the equation $|\kappa_{xx}| = 1/(1-b) + C_1$ must be non-negative, $1/(1-b) + C_1 \geq 0$. For small values of b , this leads to $C_1 \geq -1$. The only value of C_1 compatible with the last two conditions is $C_1 = -1$. Using this in (4), we arrive at the final expression for the dimensionless thickness of the surrounding annulus, as a function of capillary number,

$$b = \frac{8Ca^2}{C_2 + 40Ca^2}. \quad (5)$$

Equation (5) still contains an unknown quantity C_2 , which is the value of the function $\kappa^5 \ln^2 \kappa$ at an unknown position in the transition region between the nose of the moving meniscus and the film. It cannot be too close to the nose, though, where this function has a mathematical limit of zero, because this would violate our assumption of the small slope of the fluid-fluid interface. All we can say at this point is that C_2 is small, but its exact value cannot be deduced from the theoretical argument alone.

We have two immediate, testable physical predictions from equation (5). At relatively large capillary numbers, the film thickness b levels off at a constant value of $b = 0.2$. At small capillary numbers, it becomes proportional to Ca^2 , that is, has a constant slope of two if plotted on a log-log scale. The thickness dependence on the capillary number is therefore predicted to have a corner separating a sloping, lower- Ca , region from a constant, higher- Ca , region. The film thickness does not appear to depend on the viscosity ratio of the core and film fluids. These predictions can be tested against experiment; by fitting experimental data, the constant C_2 can be determined as well. Theories of residual film thickness for liquid-liquid invasion scenarios in core-annular flow, developed earlier [3, 16] failed to propose a similar, closed-form and testable relationship.

We would like to emphasize here in what respects our theory deviates from Bretherton's [2]. First, our theory is strictly applicable to the case of liquid-liquid displacement only. It assumes incompressibility of both phases and therefore is not expected to correctly describe the invasion of a gas bubble. A bubble is compressed in response to capillary pressure, but this effect is absent from the formulation of Laplace's law that we have used. An augmented form of Laplace's law, which would include the

compressibility effect, would incorporate the volume of the bubble, resulting in the bubble's size being controlled by the pressures in both phases (e. g., [Ref. 17, pp. 233-234]). This would make the problem even more complex. That is why our theory will only be compared to experimental results involving liquid-liquid displacement. Note that Bretherton [2] also founded his theory on the same incompressible-fluid assumption, although he compared it with experiments involving gas bubbles.

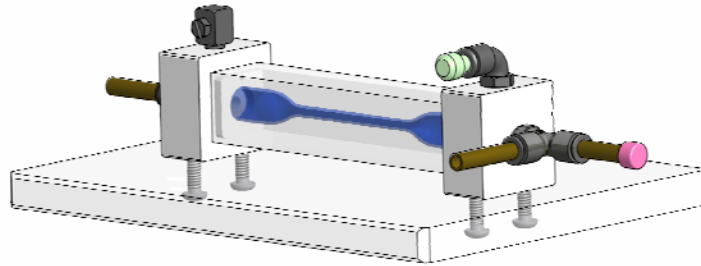
Second, Bretherton's derivation of his film-profile equation (11), performed in the assumption of a "planar" interface [Ref. 2, p. 169], neglected the transverse-curvature term $1/\kappa$ (in our notation) in the expression for the mean curvature in Laplace's law. This can be directly checked by re-deriving Bretherton's equation (9) from his equation (7). We have retained this term, important for the rendition of the cylindrical geometry. Third, Bretherton's analysis assumed a lubrication flow in the film but neglected it in the formulation of the mass balance underlying the ultimate film-thickness equation. We have chosen to use a different mass-balance formulation instead. Fourth, Bretherton made an assumption of constant, zero pressure inside the gas phase. This is also inaccurate. Bretherton's theory [Ref. 2, p. 169] assumes an inviscid bubble with zero tangential stress at the interface; therefore, there is no drag on the bubble in this model. In the absence of both the drag and an internal pressure gradient, a bubble would have no driving force to move. On the other hand, our approach uses the actual variable pressure in the core.

It is noteworthy in this regard that the validity of Bretherton's relationship, for sufficiently small capillary numbers ($\sim 5 \times 10^{-5}$ - 10^{-2}), was confirmed by direct computational-fluid-dynamics simulations [Ref. 18, Figure 3]. However, the authors' model, similarly to Bretherton's, postulated a constant zero pressure inside the moving

inviscid gas bubble. It was therefore founded on the same approximation of the reality and cannot be considered a truly independent verification. Oversimplifications made in Bretherton's theory may be an alternative reason for its departures from various experimental validations.

Experiment

An experimental apparatus was built to directly observe the displacement of the pore-filling suspending fluid by an invading liquid core phase (Figure 2). It consists of a glass capillary tube with the length of 100 mm and inner diameter of 1.14 ± 0.05 mm inside a transparent Lucite viewing box with square cross-section. The region between the viewing cell and the capillary tube is filled with glycerol to reduce optical distortion



(Color online) Figure 2. Schematic of the experimental apparatus showing the capillary tube inside the viewing box.

due to the curvature of the tube. Small ports at either end of the viewing cell provide access for feeding and removing the working fluids into or out of the capillary. At the inlet side (the right side of the picture) there are two ports: one for the annular fluid and one, covered with a rubber septum, for the injection of the core fluid. The viewing cell is

illuminated from below using a fiber-optic light source and a diffuser. Images of the capillary tube are captured at a magnification of $(11.6 \pm 0.5) \times$ approximately 75 mm downstream from the entrance of the straight test section by using a reverse-mounted 28-mm Nikon lens and bellows connected to a Photron FASTCAM APX-RS high-speed digital camera mounted above the flow cell.

Aqueous solutions of glycerol were used as suspending fluids, as listed in Table 2.

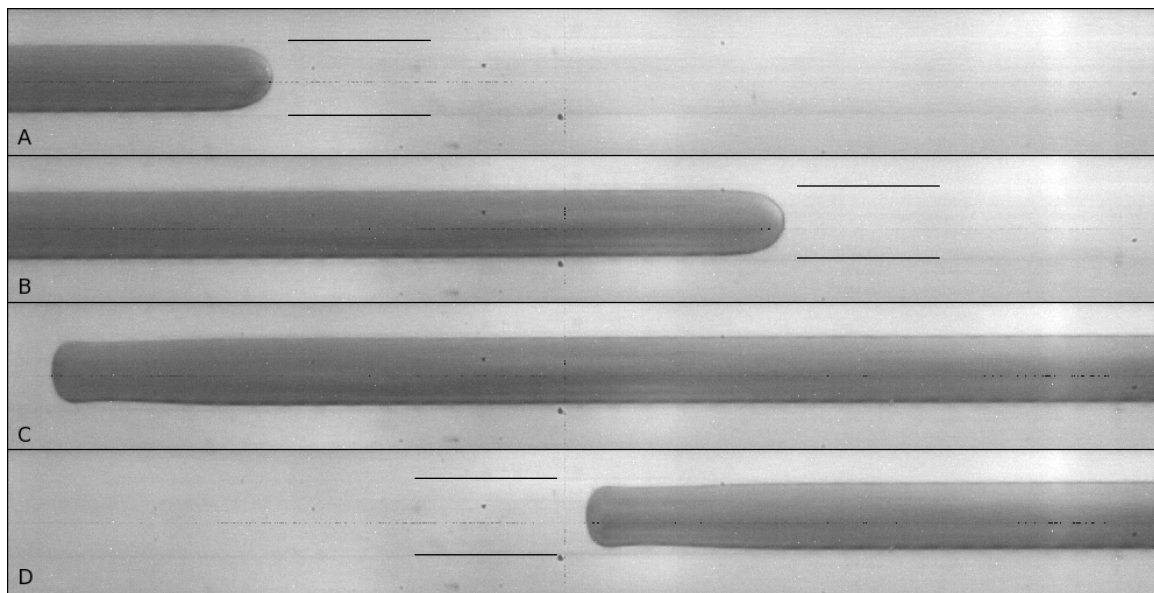


Figure 3. Series of images showing a long heptane drop invading the capillary tube filled with glycerol solution. Flow is from left to right; for this experiment, $Ca = 0.04$. The capillary wall is nearly invisible due to index-of-refraction matching between the suspending fluid and the glass; the wall edges are indicated by a pair of horizontal solid lines drawn next to the menisci. These images were obtained at low magnification (1x) to allow viewing of a large portion of the drop. At this magnification, the thin film between the dark drop and the almost invisible wall is not clearly seen. Accurate measurements of film thicknesses were obtained from images at much higher magnification (11.6x).

The core fluid was heptane dyed with Oil Blue N, with the viscosity of 3.9×10^{-3} Pa s and density of 684 kg/m^3 . The fluid-fluid interfacial tension measured with a DuNouy tensiometer was 1.5×10^{-2} N/m for all three glycerol/heptane systems studied.

To remove any organic residue and increase the hydrophilicity of the glass, the capillary was first cleaned in a NaOH-ethanol-deionized-water solution and then flushed with deionized water and dried before being sealed in the viewing cell that coupled the tube with the flow system. In a given run, the capillary was first filled with the annular fluid, and the core phase was injected upstream of the test section via a syringe. The system was allowed to equilibrate, in such a way that there was no residual flow induced by the injection of the core fluid. A syringe pump then pumped the annular fluid through the capillary tube, and recording of images took place. The recording ended when the trailing meniscus exited the test section. The drop velocity U could be controlled by changing the speed of the syringe pump.

The measurement of the film thickness in pixels was performed in a digital-image editor after the completion of the experiment. This thickness was converted to absolute units through the known optical magnification and the known camera-sensor's absolute pixel size. The film thicknesses were obtained one-to-two tube diameters from the front meniscus, where the film reached a constant thickness (Figures 3A and B). The thickness remained constant between this point and the trailing meniscus (Figures 3C and D); the total drop length was approximately 16 tube diameters. Notice from Figure 3 that both the leading and the trailing menisci maintain constant shape as they pass through the tube.

Discussion of Experimental Data

Our experimental data are tabulated in Table 3 in the rows without superscripts. The lower limit on the resolved film thickness is prescribed by the value of the magnification of the optical system. After magnification, the absolute value of one pixel is $1.46\ \mu\text{m}$, which, divided by the mean radius of the tube, gives $b = 2.55 \times 10^{-3}$ as the smallest value that we could resolve, corresponding to the thickness of one pixel. This is the smallest b listed in Table 3 for our data. The experiments run at respectively lower capillary numbers led to the film “disappearance”, meaning that its thickness fell below the limit of resolution of one pixel.

A note is in order regarding the methods that various experimenters have used to report film thicknesses in either gas-liquid or liquid-liquid displacements. Bretherton [2] and Schwartz *et al.* [3], who observed gas-bubble motion, employed the similar indirect approach, in which they observed a reduction in length of a moving liquid slug pushed by the gas phase. The film thickness was inferred from the length reduction over the distance traveled by the slug. This method can be argued to have a significant disadvantage of “not seeing” the film. For example, the authors have extended their experiments down to $\text{Ca} = 10^{-6}$ [2] and 10^{-5} [3]. Using Bretherton’s relationship and the tube radii reported, the absolute film thicknesses at these capillary numbers are expected to be on the order of 0.1 and $1\ \mu\text{m}$, respectively. On the other hand, the roughness of the glass wall in the tubes, examined directly under an electron microscope in a related study by Chen [Ref. 19, p. 344], was on the order of $1\ \mu\text{m}$. What is noteworthy is that both Bretherton [Ref. 2, Figure 4] and Schwartz *et al.* [Ref. 3, Figure 3] reported deviation of a constant-slope

behavior (on the log-log scale) in the inferred film thickness toward leveling-off to zero slope around the same $Ca = 10^{-5}$. In either case, the theoretical film thickness at this capillary number is close to $1 \mu\text{m}$, or the anticipated size of microscopic roughness of the surface. In such a situation, the amount of wetting fluid left behind can be expected to become independent of the motion of the slug, as it should be entirely controlled by the fluid collecting in the hollows of the surface. A trend towards capillary-number-independent constant value of film thickness at very small Ca was qualitatively predicted by Teletzke *et al.* [Ref. 16, Figure 5] and attributed to molecular effects. However, a simpler explanation, based on the disappearance of a continuous film because of rough surface, seems to be more natural. On the other hand, if the film could be visually observed, this difficulty of resolving a “film” if none actually existed would not arise.

Chen [19] reported film thicknesses for both gas- and liquid-liquid displacement using a different but also indirect method. The technique, borrowed from Marchessault and Mason [20], consisted in measuring electrical resistance of a capillary containing the core and film fluids. The resistance was converted into film thickness using an idealized model of an electrical conductor composed of coaxial inner and outer cylinders. A disadvantage of this technique is in its reliance on an idealized cylindrical geometry. An (unknown) increase in measured conductance is always contributed by the fluid collected in the hollows of the tube surface. This contribution becomes dominant when the size of the surface roughness is comparable to the expected thickness of the film. The inferred thickness is therefore always inaccurate and becomes virtually meaningless in the latter case. Calibration studies were not reported that could quantify the error.

Because of the increase in conductance contributed by the fluid in the roughness, the method is expected to always overpredict the true film thickness and measure a “constant” thickness at capillary numbers at which the expected thickness is comparable to the roughness size. Because the amount of overprediction grows with the decreasing capillary number, the method will also tend to diminish the true slope of the b -Ca relationship. Chen [Ref. 19, Figure 3] indeed overpredicts Bretherton’s theoretical film thickness at all capillary numbers and also reports a slope reduced compared with Bretherton’s relation. The “leveling-off” to a constant value around $Ca = 10^{-5}$ for gas invasion (which virtually coincides with the respective leveling-off Ca values reported by Bretherton and Schwartz *et al.*) and 10^{-4} for liquid invasion is also reported. For the tube radius used, Bretherton’s relationship gives the anticipated film thicknesses of approximately 0.2 and 1 μm , respectively. The depth of the hollows, estimated from electron microscopy, is 1 μm , too. The film overprediction is evident from the fact that, for stationary air bubbles, Chen [Ref. 19, p. 346] measured the film “thickness” of 0.7 μm , while it should theoretically be zero. An anomalous character of Chen’s data is also indicated by Ratulowski and Chang [Ref. 4, Figure 8]. While the authors were able to give a consistent theoretical fit, based on a single model, to the scatter of experimental results of Bretherton and Schwartz *et al.*, they could not fit Chen’s constant-slope data within the same approach. Overprediction with the electrical-resistance method is also demonstrated by the fact that Marchessault and Mason’s [20] results (as compared by Bretherton [Ref. 2, Figure 4]) consistently exceed Bretherton’s predicted film thickness at all capillary numbers as well.

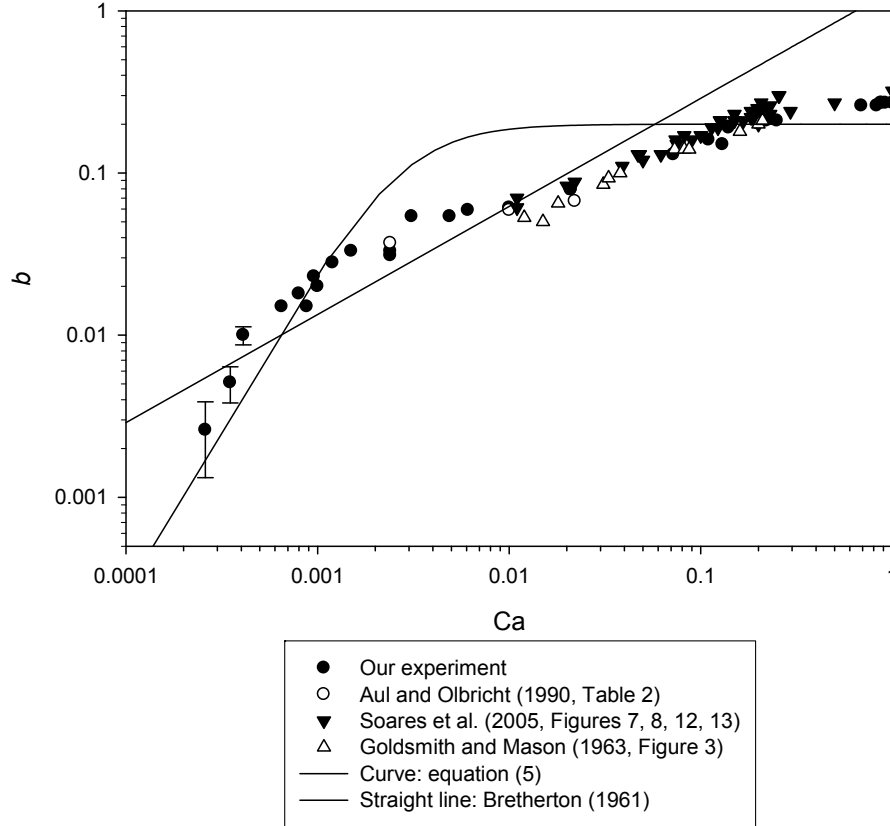


Figure 4. Summary of experimental data and theories on the wetting-film thickness versus capillary number.

For the reasons explained, we prefer to use only the data on film thicknesses in liquid-liquid invasion measured by direct film observation by optical means. Table 3 contains a compilation of such measurements in addition to ours ([Ref. 15, Figure 3; Ref. 21, Table 2; Ref. 22, Figures 7, 8, 12, 13]) (identical rows mean availability of experiments with exactly same results). All data are graphically presented in Figure 4, where the values from various authors are indicated by different symbols. For our experiments, the average uncertainty of a film-thickness measurement is 0.5 pixel, which leads to the relative error of 50 % when the thickness approaches the limit of resolution. This determines the value of the error bars for our results shown in Figure 4. Clearly, the errors grow as b decreases but are only visible, on the scale of the graph, at the three

lowest values of the capillary number; in all other cases, the errors are smaller than the circle size.

The solid curve in Figure 4 is equation (5) visually fit to all the data, with $C_2 = 3 \times 10^{-4}$. Bretherton's equation $b = 1.34 \times Ca^{2/3}$ is plotted as the solid straight line. The combined experimental data unambiguously indicate the presence of a "corner" between $Ca = 10^{-3}$ and 10^{-2} , separating the two general slopes in the observed relationship, which is missed by the application of Bretherton's single-slope theory. The low- Ca slope is correctly captured by the present theory, as well as the leveling off at $b \approx 0.3$ at the higher

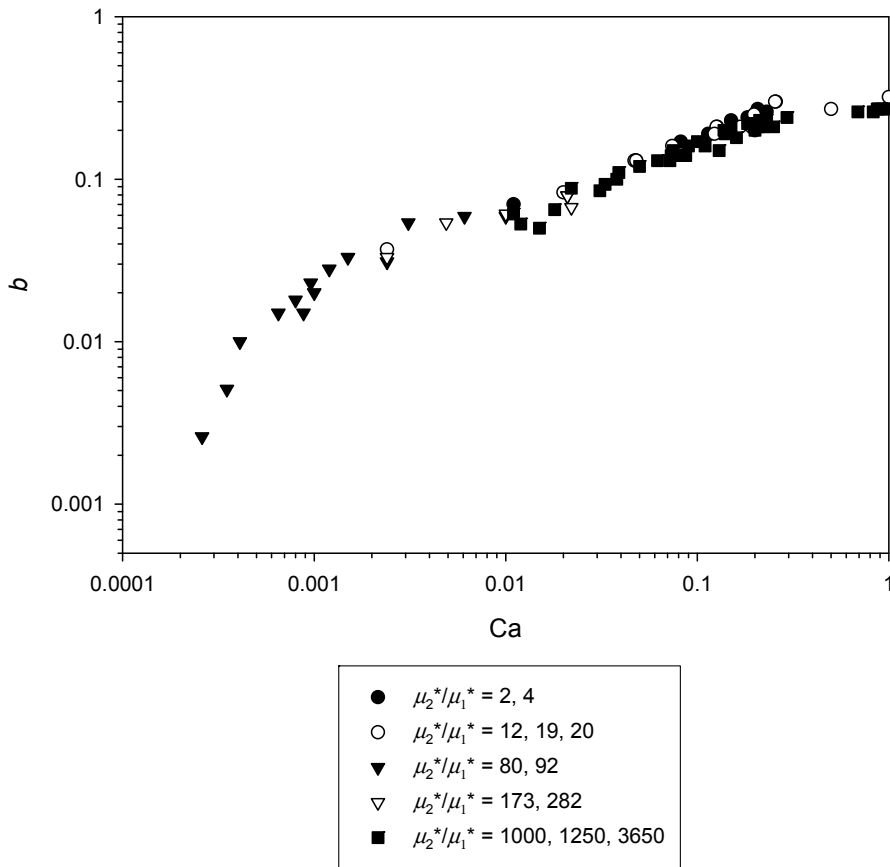


Figure 5. Data from Figure 4 coded according to viscosity ratios.

end of the capillary number. The intermediate range is captured reasonably well, with deviations of no more than a factor of 2 to 3. The data compiled from different investigations are mutually consistent, in that no systematic deviation of points of one study from another is seen.

One corollary from the present theory is an approximate independence of the film thickness of the viscosity ratio. Figure 5 presents the same data points as in Figure 4, which are coded in groups of close viscosity ratios. No systematic separation of one group from another is found, despite the fact that viscosity ratios vary by more than three orders of magnitude. Points, different in viscosity ratio by this amount, in certain instances overlap. This supports the theory's conclusion, in the range of capillary numbers tested.

The present theoretical derivation, as well as previous attempts to build such a theory, seem to indicate that, due to the complexity of the phenomenon, it is not possible to deduce a simple relationship between the annular film thickness and Ca that would be able to match experimental data with better precision in the entire capillary-number range.

Conclusions

A hydrodynamic theory of the thickness of a residual wetting film left behind during invasion of a core fluid into a capillary channel leads to equation (5). Notwithstanding the value of the constant C_2 , the theory predicts two distinct slopes in the dependence of b on capillary number, separated by a “kink”. The lower- Ca

asymptotic behavior is Ca^2 , while a constant level of $b = 0.2$ is predicted to be reached at the higher end.

We collected laboratory measurements in which the values of b for liquid-liquid invasion have been reported using direct optical observation. Direct observation is the most unambiguous method that does not infer the presence of the deposited films but rather measures them only if they realistically exist. We have also conducted our own laboratory experiment. The data, obtained by different investigators, are mutually consistent, and the theoretically predicted behavior is seen in all the data.

The only conclusion about the constant C_2 in equation (5), available from within the theory, is that it is a small number. Based on experimental data, C_2 is evaluated to be 0.0003. With this value, the film thickness in the entire range of capillary numbers available from the experiments is matched reasonably well.

It follows from the theory that the film thickness, described by equation (5), is roughly independent of the viscosity ratio between the core and film fluids. The data, coded according to viscosity ratio in Figure 5, do not show any significant scatter for the viscosity ratios changing over three orders of magnitude. This supports the theory's conclusion. Computational-fluid-dynamics simulations conducted by Soares and Thompson [Ref. 23, Figure 6] reached the same conclusion for Ca of less than approximately 0.2, while the authors computationally predicted thickening of the films with decreasing film-to-core viscosity ratios at greater capillary numbers. The data in Figure 5 do not show a clear trend toward such a behavior, although it cannot be ruled out that it may reveal itself at higher capillary numbers.

The classic theory of Bretherton [2], developed for the displacement of liquids by gas bubbles but often believed to describe the wetting films during liquid/liquid invasion, fails to capture the salient features of the experimental relationship.

Hodges *et al.* [24] proposed an asymptotic theory, seeking the dimensionless film thickness b in the form $b = F(\mu_1^* / \mu_2^*, Ca)Ca^{2/3}$. The results are presented implicitly: the function F is expressed in different asymptotic regimes defined by b itself, offering no explicit, testable predictions for b . For all small core-to-film viscosity ratios, Bretherton's relation is predicted to hold. Park and Homsy [Ref. 9, equation 4.27] also suggested that Bretherton's result extended without change to liquid-liquid invasion. Their main evolution equation (4.15), on which this conclusion is based, has the same form as Bretherton's equation (11), which allowed the authors to apply their theory to liquid-liquid invasion. However, Park and Homsy did not provide the derivation of this equation. If it is the same as Bretherton's derivation, the latter was explicitly dependent on the assumption of constant zero pressure in the core (gas) phase. This is an oversimplification, which may explain why the suggested behavior is not seen in the experiments. To fit an experimentally observed b - Ca relationship, we have used the actual variable pressure gradients in the core.

Overall, the experiments do not support the proposed extensions of Bretherton's single-slope relation to liquid-liquid invasion. Note that the present theory is not expected to be valid for invading gas bubbles, either, due to possible effects of compressibility [17].

Acknowledgments

This study was supported through the National Science Foundation (award EAR-0602556) and Petroleum Research Fund (award 45169-AC9). The authors are grateful to R. Ewing for fruitful discussions and to the two anonymous reviewers for the constructive comments.

References

- [1] S. Middleman, *Modeling axisymmetric flows* (Academic Press, San Diego, 1995).
- [2] F. P. Bretherton, *Journal of Fluid Mechanics* **10**, 166 (1961).
- [3] L. W. Schwartz, H. M. Princen, and A. D. Kiss, *Journal of Fluid Mechanics* **172**, 259 (1986).
- [4] J. Ratulowski and H.-C. Chang, *Journal of Fluid Mechanics* **210**, 303 (1990).
- [5] F. Fairbrother and A. E. Stubbs, *Journal of the Chemical Society*, 527 (1935).
- [6] G. I. Taylor, *Journal of Fluid Mechanics* **10**, 161 (1961).
- [7] D. Quéré, *Annual Review of Fluid Mechanics* **31**, 347 (1999).
- [8] T. J. Peña, M. S. Carvalho, and V. Alvarado, *AIChE Journal* **55**, 1993 (2009).
- [9] C.-W. Park and G. M. Homsy, *Journal of Fluid Mechanics* **139**, 291 (1984).
- [10] I. A. Beresnev and W. Deng, *Physics of Fluids* **22**, 012105 (2010).
- [11] P. S. Hammond, *Journal of Fluid Mechanics* **137**, 363 (1983).
- [12] G. Ooms, C. Vuik, and P. Poesio, *Physics of Fluids* **19**, 092103 (2007).
- [13] P. A. Gauglitz and C. J. Radke, *Chemical Engineering Science* **43**, 1457 (1988).
- [14] I. A. Beresnev, W. Li, and R. D. Vigil, *Transport in Porous Media* **80**, 581 (2009).
- [15] H. L. Goldsmith and S. G. Mason, *Journal of Colloid Science* **18**, 237 (1963).
- [16] G. F. Teletzke, H. T. Davis, and L. E. Scriven, *Revue de Physique Appliquée* **23**, 989 (1988).
- [17] P. A. Gauglitz and C. J. Radke, *AIChE Journal* **35**, 230 (1989).
- [18] M. D. Giavedoni and F. A. Saita, *Physics of Fluids* **9**, 2420 (1997).
- [19] J.-D. Chen, *Journal of Colloid and Interface Science* **109**, 341 (1986).

- [20] R. N. Marchessault and S. G. Mason, *Industrial and Engineering Chemistry* **52**, 79 (1960).
- [21] R. W. Aul and W. L. Olbricht, *Journal of Fluid Mechanics* **215**, 585 (1990).
- [22] E. J. Soares, M. S. Carvalho, and P. R. Souza Mendes, *Journal of Fluids Engineering* **127** (2005).
- [23] E. J. Soares and R. L. Thompson, *Journal of Fluid Mechanics* **641**, 63 (2009).
- [24] S. R. Hodges, O. E. Jensen, and J. M. Rallison, *Journal of Fluid Mechanics* **501**, 279 (2004).

Figure Captions

Figure 1. Geometry of the core-fluid invasion.

(Color online) Figure 2. Schematic of the experimental apparatus showing the capillary tube inside the viewing box.

Figure 3. Series of images showing a long heptane drop invading the capillary tube filled with glycerol solution. Flow is from left to right; for this experiment, $Ca = 0.04$. The capillary wall is nearly invisible due to index-of-refraction matching between the suspending fluid and the glass. These images were obtained at low magnification (1x) to allow viewing of a large portion of the drop. At this magnification, the thin film between the dark drop and the almost invisible wall is not clearly seen. Accurate measurements of film thicknesses were obtained from images at much higher magnification (11.6x).

Figure 4. Summary of experimental data and theories on the wetting-film thickness versus capillary number.

Figure 5. Data from Figure 4 coded according to viscosity ratios.

Table 1

Synopsis of Studies on b -Ca Behavior for Moving Gas Bubbles

Authors	Range of Ca	$b = 1.34 \times \text{Ca}^{2/3}$ or $0.5 \times \text{Ca}^{1/2}$?
Fairbrother and Stubbs [5]	10^{-4} - 10^{-2}	$0.5 \times \text{Ca}^{1/2}$
Bretherton [2]	10^{-6} - 10^{-2}	$1.34 \times \text{Ca}^{2/3}$
Schwartz <i>et al.</i> [3]	10^{-5} - 10^{-3}	Both
Ratulowski and Chang [4]	10^{-6} - 10^{-1}	Both

Table 2

Properties of the Wetting (Annulus) Fluid

Annulus Fluid	Viscosity (Pa s)	Density (kg/m ³)
Glycerol 100% wt	1.4	1260
Glycerol 85% wt	0.11	1220
Glycerol 75% wt	0.036	1170

Table 3

Experimental Data on Wetting-Film Thickness for Liquid-Liquid Invasion

Ca	b	μ_2^* / μ_1^*
0.00026	0.0026	92
0.00035	0.0051	92
0.00041	0.010	92
0.00065	0.015	92
0.00080	0.018	92
0.00088	0.015	92
0.00096	0.023	92
0.0010	0.020	92
0.0012	0.028	92
0.0015	0.033	92
0.0024	0.031	92
0.0024	0.033	282
0.0024 [†]	0.037 [†]	19 [†]
0.0031	0.054	92
0.0049	0.054	282
0.0061	0.059	92
0.010	0.061	282
0.010 [†]	0.059 [†]	80 [†]
0.011 [*]	0.061 [*]	1000 [*]
0.011 [*]	0.070 [*]	4 [*]
0.012 [‡]	0.053 [‡]	1250 [‡]
0.015 [‡]	0.050 [‡]	1250 [‡]
0.018 [‡]	0.065 [‡]	1250 [‡]
0.020 [*]	0.083 [*]	20 [*]
0.021	0.079	282
0.021	0.079	282
0.022 [†]	0.067 [†]	173 [†]
0.022 [*]	0.088 [*]	1000 [*]
0.031 [‡]	0.085 [‡]	1250 [‡]
0.033 [‡]	0.093 [‡]	1250 [‡]
0.038 [‡]	0.10 [‡]	1250 [‡]
0.039 [*]	0.11 [*]	1000 [*]
0.047 [*]	0.13 [*]	20 [*]
0.048 [*]	0.13 [*]	12 [*]
0.048 [*]	0.13 [*]	2 [*]
0.050 [*]	0.12 [*]	1000 [*]
0.062 [*]	0.13 [*]	1000 [*]
0.072	0.13	3650
0.073 [‡]	0.14 [‡]	1250 [‡]
0.074 [*]	0.16 [*]	12 [*]

0.075*	0.15*	1000*
0.082*	0.17*	4*
0.082‡	0.14‡	1250‡
0.087‡	0.14‡	1250‡
0.090*	0.16*	1000*
0.100*	0.17*	1000*
0.11	0.16	3650
0.11*	0.19*	4*
0.12*	0.19*	12*
0.13	0.15	3650
0.13*	0.21*	2*
0.13*	0.21*	20*
0.14*	0.20*	1000*
0.14	0.19	3650
0.15*	0.21*	1000*
0.15*	0.23*	2*
0.16‡	0.18‡	1250‡
0.17*	0.21*	12*
0.18*	0.22*	1000*
0.18*	0.24*	4*
0.19*	0.22*	1000*
0.19*	0.21*	12*
0.19*	0.24*	4*
0.20	0.21	3650
0.20*	0.20*	20*
0.20*	0.25*	20*
0.20*	0.21*	12*
0.20*	0.23*	4*
0.20*	0.24*	2*
0.20‡	0.20‡	1250‡
0.21*	0.23*	1000*
0.21*	0.25*	4*
0.21*	0.27*	2*
0.21‡	0.21‡	1250‡
0.22	0.21	3650
0.23*	0.23*	1000*
0.23*	0.26*	4*
0.25	0.21	3650
0.26*	0.30*	2*
0.29*	0.24*	1000*
0.50*	0.27*	20*
0.69	0.26	3650
0.83	0.26	3650
0.87	0.27	3650
0.88	0.27	3650
0.92	0.27	3650

1.0	0.27	3650
1.0*	0.32*	20*

* Data from Soares *et al.* [Ref. 22, Figures 7, 8, 12, 13]

† Data from Aul and Olbricht [Ref. 21, Table 2]

‡ Data from Goldsmith and Mason [Ref. 15, Figure 3]

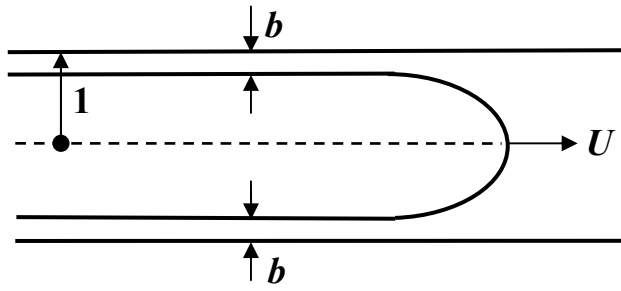
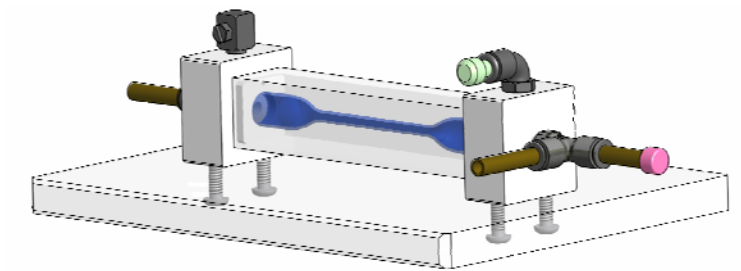


Figure 1. Geometry of the core-fluid invasion.



(Color online) Figure 2. Schematic of the experimental apparatus showing the capillary tube inside the viewing box.

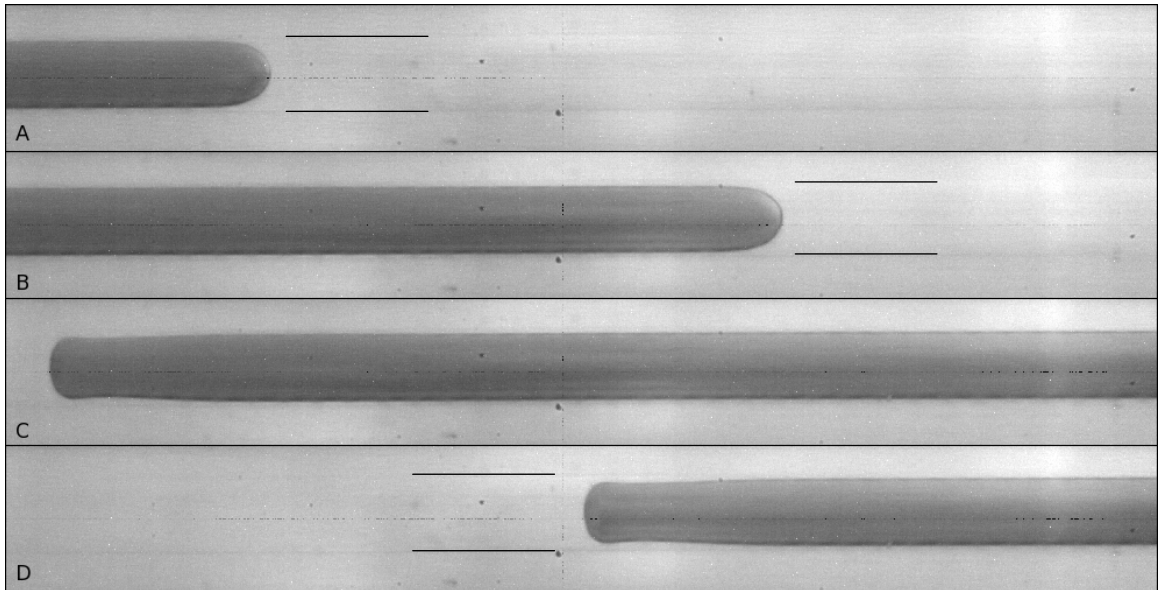


Figure 3. Series of images showing a long heptane drop invading the capillary tube filled with glycerol solution. Flow is from left to right; for this experiment, $Ca = 0.04$. The capillary wall is nearly invisible due to index-of-refraction matching between the suspending fluid and the glass; the wall edges are indicated by a pair of horizontal solid lines drawn next to the menisci. These images were obtained at low magnification (1x) to allow viewing of a large portion of the drop. At this magnification, the thin film between the dark drop and the almost invisible wall is not clearly seen. Accurate measurements of film thicknesses were obtained from images at much higher magnification (11.6x).

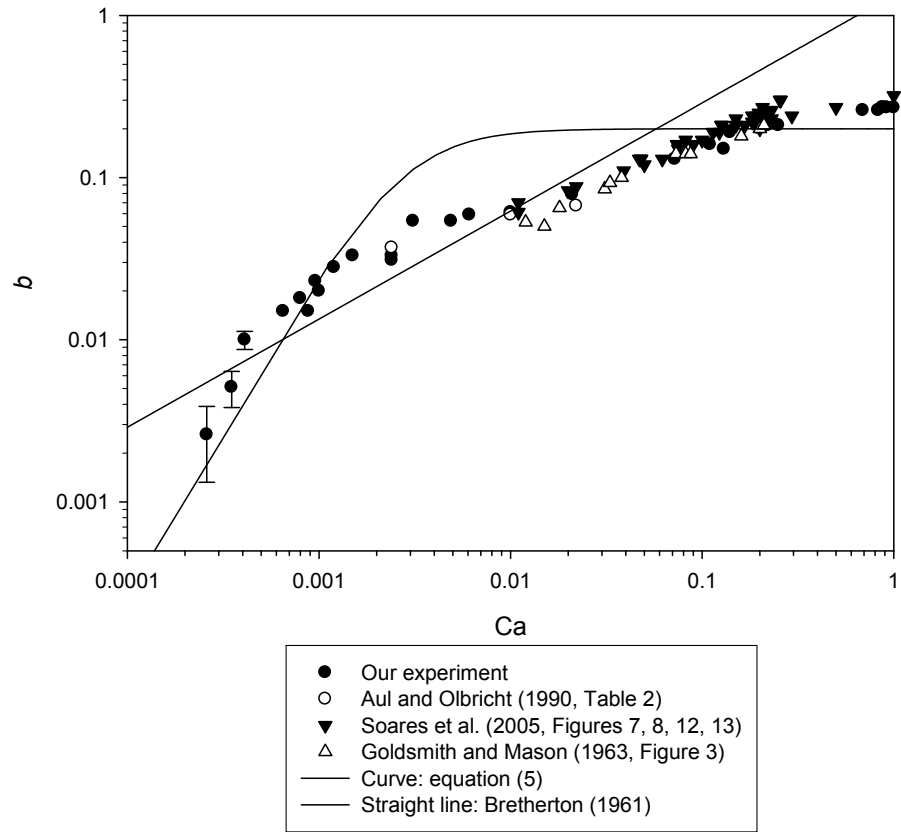


Figure 4. Summary of experimental data and theories on the wetting-film thickness versus capillary number.

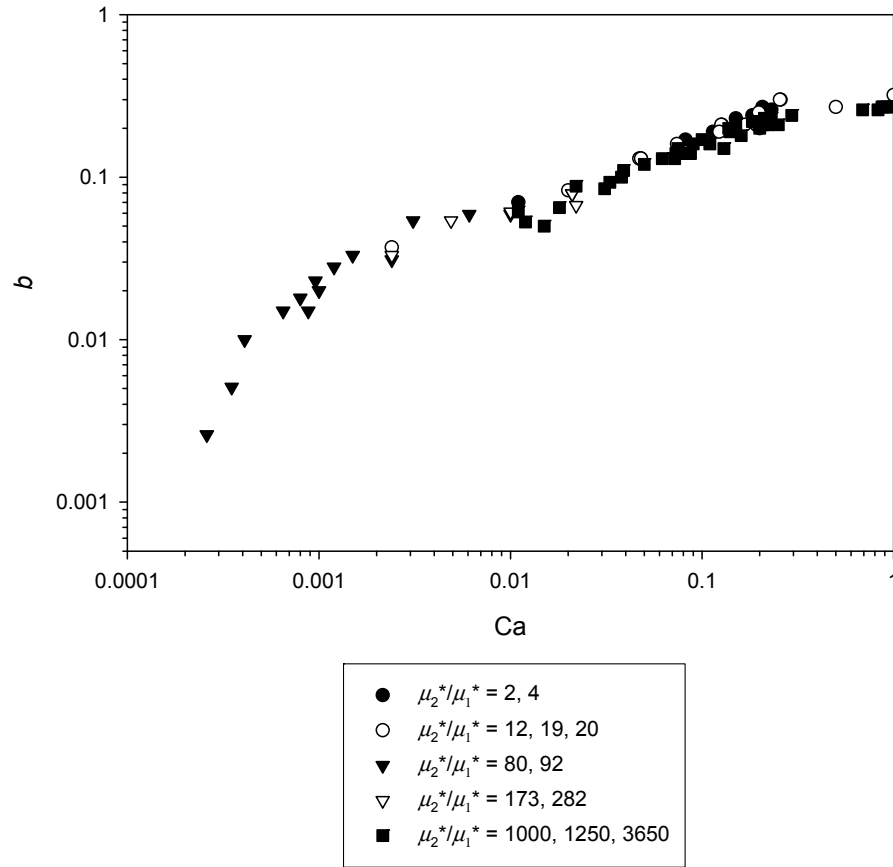


Figure 5. Data from Figure 4 coded according to viscosity ratios.